

# Asymptotic statistics of the $n$ -sided planar Poisson-Voronoi cell: II. Heuristics

H. J. Hilhorst

Laboratoire de Physique Théorique, Bâtiment 210  
Université Paris-Sud XI and CNRS  
91405 Orsay Cedex, France

February 3, 2022

## Abstract

We develop a set of heuristic arguments to explain several results on planar Poisson-Voronoi tessellations that were derived earlier at the cost of considerable mathematical effort. The results concern Voronoi cells having a large number  $n$  of sides. The arguments start from an entropy balance applied to the arrangement of  $n$  neighbors around a central cell. It is followed by a simplified evaluation of the phase space integral for the probability  $p_n$  that an arbitrary cell be  $n$ -sided. The limitations of the arguments are indicated. As a new application we calculate the expected number of Gabriel (or full) neighbors of an  $n$ -sided cell in the large- $n$  limit.

**Keywords:** planar Voronoi cell, sidedness, Gabriel neighbors

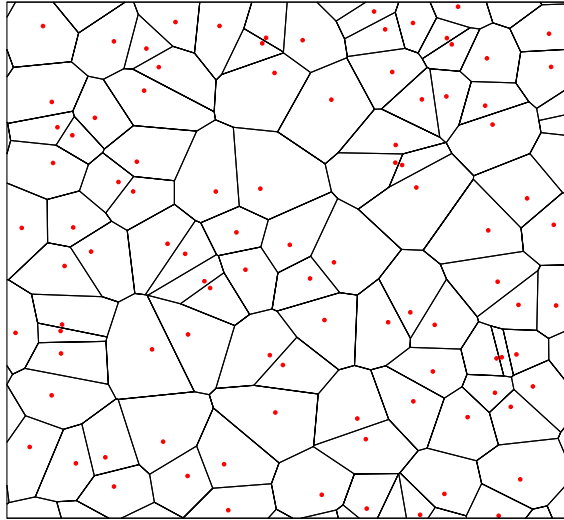


Figure 1: Voronoi tessellation of a set of point particles. Voronoi cells are convex and their edges join at trivalent vertices.

## 1 Introduction

Planar cellular structures occur in a wide variety of natural systems. The examples most quoted are certain biological tissues and soap froths confined between parallel plates. In addition, cellular structures are employed as a tool of analysis in a great diversity of problems throughout the sciences and beyond. Many references may be found *e.g.* in Okabe *et al.* [1] and in Rivier [2].

The *Voronoi tessellation* is one of the simplest mathematical models of a cellular structure. In two dimensions it is obtained by distributing a set of point-like “seeds” in the plane and then performing the Voronoi construction as in the example of Fig. 1: the plane is partitioned into cells such that each point of the plane is in the cell of the seed to which it is closest. Voronoi cells are convex and their edges join at trivalent vertices. In the special case that the seed positions are drawn randomly from a uniform distribution, one speaks of a *Poisson-Voronoi* tessellation.

The statistical properties of the Poisson-Voronoi tessellation were studied by Meijering [3] as early as 1953. Among the quantities of greatest interest is the *sidedness probability*  $p_n$ , defined as the fraction of cells that are  $n$ -sided ( $n = 3, 4, 5, \dots$ ). As  $n$  increases,  $p_n$  passes through a maximum at  $n = 6$  and falls off to zero very rapidly for  $n \gtrsim 10$ . The statistical properties of Voronoi cells range from fairly easy to very hard to determine, depending on the quantity of interest. Many known properties are discussed and/or listed in Ref. [1] (see, *e.g.*, Ch. 5, Table 5.5.1).

It so happens that the sidedness probability  $p_n$  is very hard to calculate. Although it may readily be represented as a  $2n$ -dimensional integral, the variables of integration are coupled in such a way that this is a true many-particle problem. As a result, no simple analytic result for  $p_n$  is known for any  $n$ . We showed earlier, however, that progress can be made if one considers the limit of large  $n$ . In that limit  $p_n$  is given by [4, 5]

$$p_n = \frac{C}{4\pi^2} \frac{(8\pi^2)^n}{(2n)!} [1 + o(1)], \quad n \rightarrow \infty, \quad (1.1)$$

where  $C = 0.344\,347\dots$  [6]. Alternatively Eq. (1.1) may be written

$$\log p_n = -2n \log n + n \log(2\pi^2 e^2) - \frac{1}{2} \log n - \frac{1}{2} \log(2^6 \pi^5 C^{-2}) + o(1). \quad (1.2)$$

The interest of this asymptotic result, obtained by lengthy and technical mathematics, goes much beyond the formula itself. Its derivation has brought along a full analysis of the configurational statistics of the  $n$ -sided cell, which in turn has opened the door to further developments in various directions that we will briefly mention now.

(i) First, let  $m_n$  be the average sidedness of the *neighbor* of an  $n$ -sided cell. In the wake of the work of Ref. [5] it was shown [7] that this sidedness pair correlation has the large- $n$  expansion  $m_n = 4 + 3\pi^{\frac{1}{2}} n^{-\frac{1}{2}} + \dots$ . This demonstrated that Aboav's celebrated law [8], usually written as  $nm_n = an + b$ , is in fact a linear approximation useful for, but limited to, small  $n$  values.

(ii) Secondly, the development of a new Monte Carlo method [9] made it possible to simulate  $n$ -sided cells and to numerically determine  $p_n$  with four-digit precision for all finite values of  $n$ . This method was used to generate snapshots of extremely large cells with sidednesses as high as  $n = 1600$  [10].

(iii) Thirdly, the analytic methods developed for Voronoi cells in Refs. [4, 5] proved to be of wider use. In Ref. [11] they were applied to line tessellations of the plane and linked up with work in mathematics by Hug and Schneider [12]. In Ref. [13] they were brought to bear on *Sylvester's question* [14]: what is the probability  $p_n^*$  that  $n$  points chosen randomly from a uniform distribution in a disk, are the vertices of an  $n$ -sided convex polygon? This question leads to a connection between on the one hand our studies of many-sided Voronoi cells, and on the other hand work on random points in convex position by Bárány [15], Bárány *et al.* [16], and Calka and Schreiber [17], as well as work in statistical physics on extremal statistics of random walks by Györgyi *et al.* [18] and Majumdar and Comtet [19, 20].

Because of all these ramifications we are justified to ask which of the results on many-sided Voronoi cells can be understood without the full mathematical apparatus that was necessary in Ref. [5] and in most of the following

articles. This paper answers that question. It is a successor to Ref. [5], of which we will reproduce part of the results by new, elementary but heuristic arguments. We also indicate the limitations of these arguments. Finally, the present paper will lay the basis for a study of Voronoi cells in higher spatial dimensions [21].

Our presentation is as follows. A preliminary observation in section 2 has to do with the difference between the statistics of *large* and of *many-sided* cells. We then estimate  $p_n$  in two successive stages. First, in section 3, and considering the many-sided cell as circular, we present heuristic arguments leading to the simplest of all possible estimates. Secondly, in section 4, and building on what we have learned, we perform part of the mathematics of Ref. [5] in a strongly simplified way. This leads to a much improved estimate of  $p_n$ .

In section 5 we consider an effect not captured by the preceding arguments, namely the “elastic” deformations of the cell perimeter from circularity. The key to their analysis is the so-called “random acceleration process,” also known from the theory of Brownian motion. We derive the scaling with  $n$  of the elastic deformations; it is not possible, however, to obtain heuristically their precise contribution to  $p_n$ .

In section 5.3, finally, we consider the average number of Gabriel neighbors of an  $n$ -sided cell and show that for large  $n$  it scales as  $\sim n^{\frac{1}{2}}$ . Adjacent Voronoi cells are called Gabriel neighbors when the line segment that connects their seeds does not intersect a third cell. Gabriel neighbors have been studied in mathematics [22, 23] and also play an important role in certain pattern recognition algorithms where “decision boundaries” must be constructed [24, 25]. Section 6 is our conclusion.

## 2 A preliminary observation

We consider a Poisson-Voronoi tessellation with seed density  $\rho$ ; a measure for the typical interparticle distance is therefore  $\ell_{\text{ip}} = \rho^{-\frac{1}{2}}$ . For all questions of interest this density may be scaled to unity, but we will keep it as a check on dimensionality. We select an arbitrary seed, let its position be the origin, and are interested in its Voronoi cell, which we will call the “central cell.” This cell has the same statistical properties as all others. Our focus is, first of all, on its sidedness probability  $p_n$ .

### 2.1 Large cells

It is useful to begin by pointing out a distinction. When the central cell is *large*, in the sense of having a large area, it will also typically have many sides, and inversely. Nevertheless, the statistical subensemble of central cells

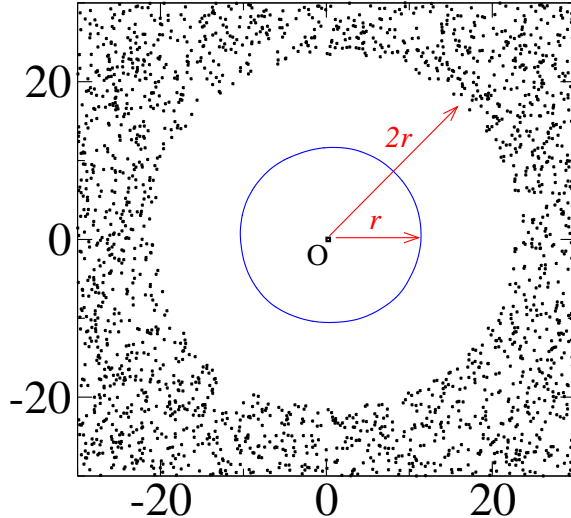


Figure 2: Black dots: seeds randomly distributed in the plane with an *a priori* uniform density  $\rho = 1$ . The picture shows a very low-probability configuration consisting of a seed in the origin surrounded by a disk of radius  $2r$  void of other seeds. The Voronoi cell of the central seed will be a convex  $n_r$ -sided polygon, where  $n_r$  is a random number of order  $r^{\frac{2}{3}}$ . The cell perimeter will roughly coincide with the circle of radius  $r$  shown in the figure.

with a prescribed area  $A$  is inequivalent to the one where it has a prescribed number  $n$  of sides, even in the limit of large  $A$  and  $n$ . We will now discuss why.

Let us first ask how it can happen that the central cell (say an approximately circular one [26]) has a large area  $A = \pi r^2$ . As shown in Fig. 2, this occurs when a disk of radius  $2r$  around the central seed is free of other seeds. Now let us inquire about the sidedness  $n_r$  of this large cell, or, equivalently, its number of first-neighbor cells. One might think naively that in the limit of large  $r$  this number can be estimated as the product of the seed density  $\rho$  and the area of an annulus of width  $\ell_{\text{ip}}$  along the perimeter of the empty disk. That would give  $n_r \sim \rho \times \ell_{\text{ip}} \times 4\pi r \sim \rho^{\frac{1}{2}} r$ , where the sign  $\sim$  denotes asymptotic proportionality as  $r$  gets large. The Voronoi construction, however, does not confirm this linearity between  $n_r$  and  $r$ . Thanks to work by Calka [28] and Calka and Schreiber [17] we know that in fact the number of first neighbors increases only as  $n_r \sim (\rho^{\frac{1}{2}} r)^{\frac{2}{3}}$  and that they are essentially located in a circular annulus of width  $\sim \rho^{-\frac{2}{3}} r^{-\frac{1}{3}}$  along the perimeter of the empty disk. The cause is a screening effect that we will study in detail in section 3.1.

## 2.2 Constructing a many-sided cell

Obtaining an  $n$ -sided cell by the construction of Fig. 2 would require having an empty disk of radius  $2r$  such that  $n_r = n$ , and hence would require  $r \sim r_n \equiv \rho^{-\frac{1}{2}} n^{\frac{3}{2}}$ . The probability for this to happen is  $\exp(-\pi \rho r_n^2) = \exp(-\text{cst} \times n^3)$ , which with respect to an arbitrary seed distribution corresponds to an entropy loss  $\Delta S$  equal to [29]

$$\Delta S \sim -n^3, \quad n \rightarrow \infty. \quad (2.1)$$

It then becomes clear that perhaps there is a way of creating an  $n$ -sided central cell at lower entropy cost. If the annulus with the  $n$  first neighbors is contracted homothetically, the central cell remains  $n$ -sided. The reduction of the annular surface costs entropy but there is a compensation due to the extra space that becomes available to the seeds outside the annulus. In the next section we will obtain the maximum-entropy arrangement by balancing these two effects against each other in what may be called an *entropy-versus-entropy* argument.

## 3 Heuristic estimate for $p_n$

In order to heuristically estimate the sidedness probability  $p_n$  we proceed in two stages: a description of the screening effect in section 3.1 and an entropy balance in section 3.2.

### 3.1 Screening

Fig. 3 shows the central seed in  $O$  together with five of its first-neighbor seeds located at  $P_1, \dots, P_5$ . By constructing in the “mid-points”  $R_1, \dots, R_5$  the perpendicular bisectors of  $OP_1, \dots, OP_5$  one obtains five segments of the perimeter of the central cell. The positions of the vertices  $S_2, \dots, S_5$  then follow as indicated in Fig. 4. We will refer to the line interval  $S_m S_{m+1}$  as the  $m$ th perimeter segment (with cyclic boundary conditions,  $S_{n+1} \equiv S_1$ ). Obviously, integrating over the  $n$  nearest-neighbor positions  $P_1, \dots, P_n$  is the same thing, apart from trivial factors 2, as integrating over the  $n$  mid-point positions  $R_1, \dots, R_n$ .

We ask now the following question: what is the area available to an arbitrary seed if all other seed positions as well as the number  $n$  of perimeter segments are kept fixed? Specifically, let us study in Fig. 4 how  $R_3$  can move around when  $R_1, R_2, R_4, R_5$  are fixed. Both the polar angle and the length of the vector  $OR_3$  may vary, but  $S_3 S_4$  should stay perpendicular to this vector. The domain of variation of  $R_3$  is, clearly, determined by the condition that the intersection points  $S_3$  and  $S_4$  remain confined to the immobile intervals  $S_2 T$  and  $S_5 T$ , respectively. Some reflection then shows that  $R_3$  is restricted

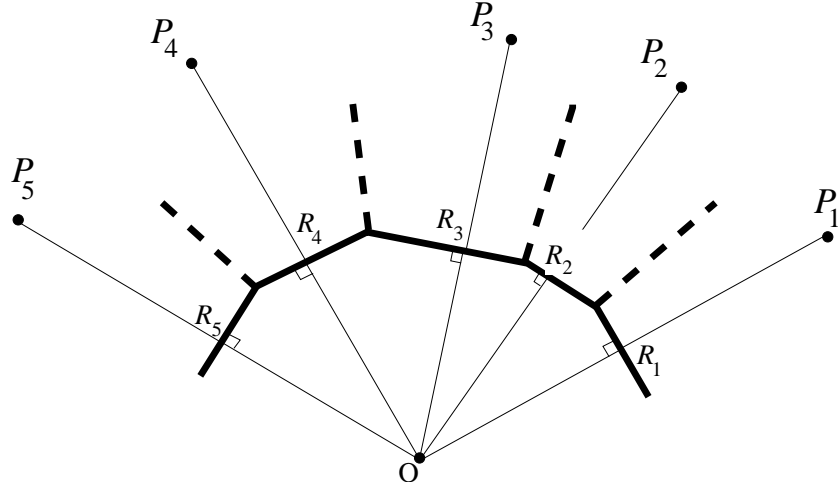


Figure 3: A central seed located in the origin  $O$  and five of its neighboring seeds at positions  $P_1, \dots, P_5$ . The “mid-points”  $R_1, \dots, R_5$  are the centers of the intervals  $OP_1, \dots, OP_5$ . Heavy solid line: part of the perimeter of the central Voronoi cell. Heavy dashed lines: boundaries between the first-neighbor Voronoi cells.

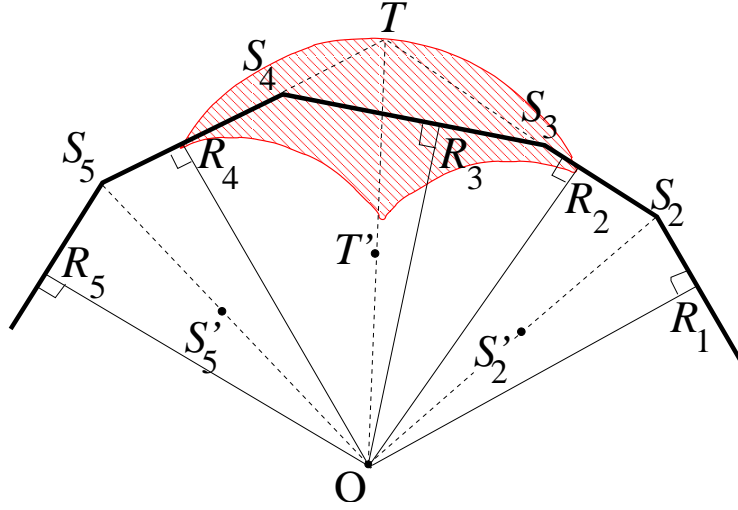


Figure 4: Heavy solid line: same part of the perimeter of the central Voronoi cell as shown in Fig. 3. The vertices are denoted  $S_2, \dots, S_5$ ; point  $T$  is a virtual vertex: it would be there if the perimeter segment  $S_3S_4$  were absent. The shaded region is the area available to mid-point  $R_3$  when all other mid-points remain fixed and the number of cell sides is not allowed to change. This region is bounded by three circular arcs; the circles pass through the origin and have their centers in  $S'_2$ ,  $T'$ , and  $S'_5$  halfway the intervals  $OS_2$ ,  $OT$ , and  $OS_5$ , respectively.

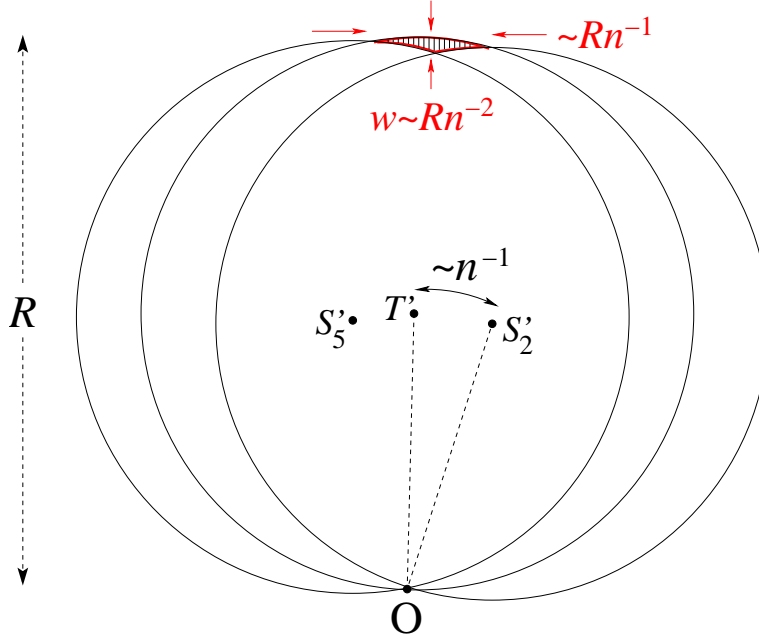


Figure 5: The three circles whose arcs were shown in Fig. 4, are represented here in full and for much larger  $n$ . Their diameters are approximately equal to  $R$  and their centers form angles of order  $n^{-1}$  with the origin. In the limit of large  $n$  the shaded area becomes triangular with two acute angles of order  $n^{-1}$ .

to the shaded region in Fig. 4. This region is bounded by three arcs of circles centered at points  $S'_2$ ,  $T'$ , and  $S'_5$  which are located halfway between the origin and the corresponding vertices. The exact surface area of the shaded region may be expressed in terms of the mid-point coordinates, but we will not need that much detail.

In the limit of large  $n$ , shown in Fig. 5, the angles  $S'_2OT'$  and  $S'_5OT'$  will typically be of order  $n^{-1}$ . The three circles have been represented in full in this figure. Let  $R$  be their typical diameter (which is also the *radius* of the central cell). One easily shows that for large  $n$  the shaded area tends towards a triangle with a long side of order  $Rn^{-1}$  and two acute angles of order  $n^{-1}$ . It follows that the triangle height  $w$  scales as

$$w \sim Rn^{-2}, \quad n \rightarrow \infty. \quad (3.1)$$

This equation expresses the screening effect: the larger  $n$ , the narrower the annulus containing the  $n$  points. We will make essential use of relation (3.1) in the subsection 3.2. It is worth noting the following consequence. The shaded area in Fig. 4 shows that when the polar angle of  $R_3$  approaches the one of  $R_2$  or  $R_4$ , the available phase space goes to zero linearly in the angle difference. This means that the screening leads to an *effective repulsion*



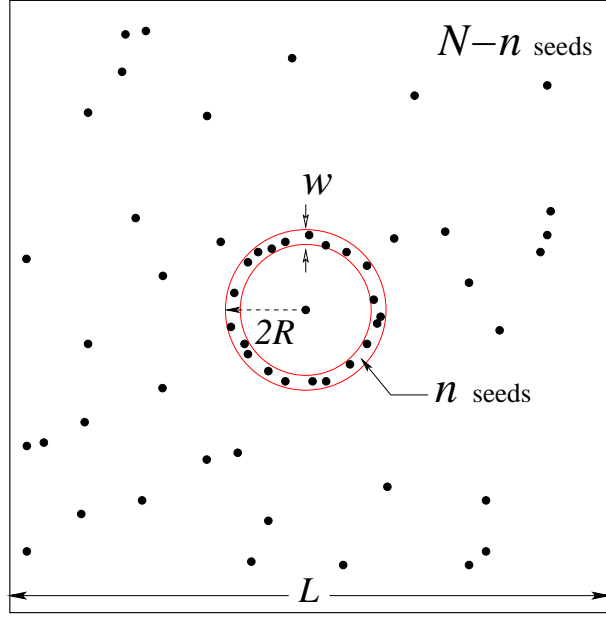


Figure 6: Given an annulus of outer radius  $2R$  and width  $w$  surrounding a central seed, we ask for the probability that out of  $N$  other seeds in an area  $L^2$ , there be none in the inner disk of radius  $2R - w$  and exactly  $n$  inside the annulus, the remaining ones occupying the outer region.

between the mid-points, an effect that will be made more quantitative in section 4.

### 3.2 Entropy balance

The considerations above suggest the next question. We consider a central seed in the origin and  $N$  others in an area  $L \times L$ . At a suitable point we will let  $N, L \rightarrow \infty$  with  $\rho \equiv N/L^2$  fixed. We now ask what the probability is for the seed configuration to be constrained as illustrated in Fig. 6: of all seeds,  $n$  are located in an annulus of outer radius  $2R$  and width  $w$ , and the remaining ones are all outside of this annulus. This probability will be our approximation for the sidedness probability  $p_n$  defined above and we will denote it by the same symbol  $p_n$ . We may write it as the exponential of an entropy difference,

$$p_n = e^{S' - S} = e^{\Delta S}, \quad (3.2)$$

where  $S'$  and  $S$  are the entropies of the constrained and unconstrained seed configuration, respectively. Let  $a_1$  and  $a_2$  denote the area of the annulus and the area of the inner disk plus annulus, respectively. As functions of the two

lengths  $R$  and  $w$  they read

$$\begin{aligned} a_1 &= \pi(2R)^2 - \pi(2R - w)^2, \\ a_2 &= \pi(2R)^2. \end{aligned} \quad (3.3)$$

In terms of these two areas we have

$$e^S = V^N, \quad e^{S'} = \binom{N}{n} (L^2 - a_2)^{N-n} a_1^n. \quad (3.4)$$

Using (3.4) in (3.2) and taking the limit  $N, L \rightarrow \infty$  as stated we get

$$p_n = \frac{(\rho a_1)^n}{n!} e^{-\rho a_2}. \quad (3.5)$$

Taking the logarithm of (3.5) and using (3.3) we obtain

$$\begin{aligned} \log p_n &= -\log n! + n \log \rho a_1 - \rho a_2 \\ &= -\log n! + n \log [\rho \pi w(4R - w)] - \rho \pi (2R)^2. \end{aligned} \quad (3.6)$$

At this point we will take into account the screening effect. Motivated by the discussion of section 3.1 we impose that  $w = 2cRn^{-2}$ , where  $c$  is a numerical constant. This ensures in some average sense that the seeds in the annulus are not screening each other. Eliminating  $w$  from (3.6) in favor of  $R$  and  $n$  we find

$$\log p_n = -\log n! + n \log(8\pi \rho c R^2 n^{-2}) - 4\pi \rho R^2 + \mathcal{O}(n^{-1}), \quad (3.7)$$

valid in the limit  $n \rightarrow \infty$ . Eq. (3.7) represents the entropy loss associated with the constraints on the seed positions. The only freedom that we have left is to choose the relation between  $R$  and  $n$ . Varying (3.7) with respect to  $R$  shows that it has a minimum for  $R = R^*$ , where

$$R^* = \left( \frac{n}{4\pi \rho} \right)^{\frac{1}{2}}. \quad (3.8)$$

This expression for  $R^*$ , obtained here heuristically, coincides with the exact result of Refs. [4, 5] for the radius  $R_c$  of the  $n$ -sided Voronoi cell. The annular width  $w^*$  corresponding to the maximum entropy is obtained by substitution of (3.8) in (3.1),

$$w^* = c(\pi \rho)^{-\frac{1}{2}} n^{-\frac{3}{2}}. \quad (3.9)$$

Eqs. (3.8) and (3.9) show that as  $n$  grows, the radius  $2R^*$  of the annulus of first-neighbor seeds increases but its width  $w^*$  decreases. The typical distance  $\ell^*$  between two adjacent first neighbors along this circle is  $\ell^* = 4\pi R^*/n = (4\pi/\rho n)^{\frac{1}{2}} \sim n^{-\frac{1}{2}}$ . From the fact that  $w^* \sim n^{-\frac{3}{2}}$  and hence

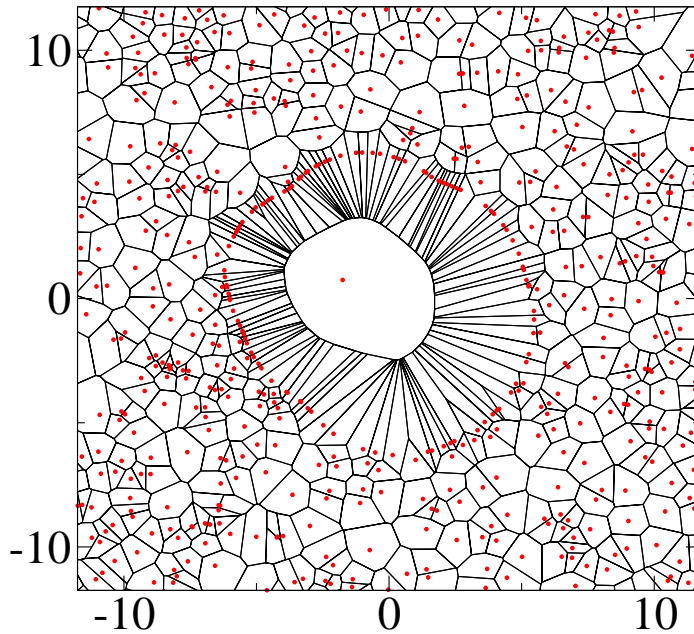


Figure 7: A Poisson-Voronoi tessellation containing a cell of  $n = 96$  sides. The seed density is  $\rho = 1$ . One clearly distinguishes the alignment of the first-neighbor seeds along an almost continuous curve. The deviations of this curve from circularity (see section 5), predicted to disappear when  $n \rightarrow \infty$ , are still important for this value of  $n$ .

$w^* \ll \ell^* \ll 1$  it follows that in the large  $n$  limit the first order neighbors align along an almost continuous curve. This is confirmed by independent Monte Carlo simulation according to the method of Ref. [9]. Fig. 7 shows a Poisson-Voronoi tessellation containing a 96-sided cell. The alignment of the first-neighbor seeds is clearly visible. This figure shows still another feature of such a large Voronoi cell: although the cell itself is convex, this need not be the case for curve of alignment of the first-neighbor seed positions.

This is also the suitable place for another side comment. When the “seeds” are physical particles having some nonzero diameter  $a$ , obviously the present considerations cease to be valid when the density of particles becomes too high. From the preceding discussion it is clear that an appropriate criterion for their validity is that  $a \ll \ell^*$ . This point was briefly discussed in Ref. [30].

To complete the calculation of this section we determine the expression for the sidedness probability as given by the present approximation. Substitution of (3.8) in (3.7) gives

$$\begin{aligned} \log p_n &= -\log n! + n \log 2cn^{-1} - n + \dots \\ &= -2n \log n + n \log 2c - \frac{1}{2} \log n - \frac{1}{2} \log 2\pi + \dots, \end{aligned} \quad (3.10)$$

in which the dot terms vanish as  $n \rightarrow \infty$ .

We now compare Eq. (3.10) to the exact expansion (1.2). The leading order term of (3.10) is correct and this is the first time that a heuristic argument achieves this. We recall that Drouffe and Itzykson [31, 32] derived the lower bound  $p_n = -\alpha n \log n + \dots$  with  $\alpha \leq 2$ ; their conjecture was that  $\alpha = 2$ , which we now know [4, 5] to be correct [6]. The second term in expansion (3.10) differs from the exact result (1.2). Indeed, obtaining this second term correctly requires a more detailed study of the arrangement of the  $n$  seeds in the annulus. This will be the subject of section 4.

## 4 Improved estimate for $p_n$

Building on the experience gained above we can now greatly improve upon the calculation of  $p_n$ . In this section  $\mathbf{P}_m$  will denote the position vector of the  $m$ th first-neighbor seed and  $P_m \equiv |\mathbf{P}_m|$  will stand for its length, with  $m = 1, 2, \dots, n$ . All exact work on  $p_n$  should start from the  $2n$ -fold phase space integral

$$p_n = \frac{\rho^n}{n!} \int d\mathbf{P}_1 \dots d\mathbf{P}_n \chi e^{-\rho\mathcal{A}}, \quad (4.1)$$

where  $\chi = 1$  (or  $\chi = 0$ ) if the condition for the  $n$  seed positions  $\mathbf{P}_m$  to each contribute a perimeter segment is satisfied (or not satisfied); and where  $\mathcal{A}$  is the area from which the remaining seeds must be excluded in order not to interfere with this  $n$ -sided cell. In this section we will evaluate (4.1) in an approximation suggested by the considerations of section 3. The expression  $\chi \exp(-\rho\mathcal{A})$  is a complicated function of the variables of integration that we will not need in detail in the present approach.

### 4.1 The $2n$ -fold integral for $p_n$

We assume that for large  $n$  the shape of the  $n$ -sided Voronoi cell will be close to a circle. Let a new variable  $P$  denote twice this circle's radius and hence be representative of the linear scale of the cell. We can then split the  $2n$ -fold integration in (4.1) into a single one on  $P$  and a set of  $2n - 1$  integrations that define the detailed shape and the orientation of the cell. For this set we will take the  $n$  polar angles of the  $\mathbf{P}_m$  and the  $n - 1$  independent ratios  $P_m/P_{m-1}$ ,  $m = 2, \dots, n$  of their radial distances. These ratios may in turn be expressed in terms of angular variables. Assuming that with negligible error we may factorize the integral on  $P$ , to be denoted  $I_{\text{rad}}$ , and the angular ones, we then have

$$p_n = \frac{1}{n!} I_{\text{rad}} I_{\text{ang}}, \quad (4.2)$$

in which we will consider  $I_{\text{rad}}$  and  $I_{\text{ang}}$  separately.

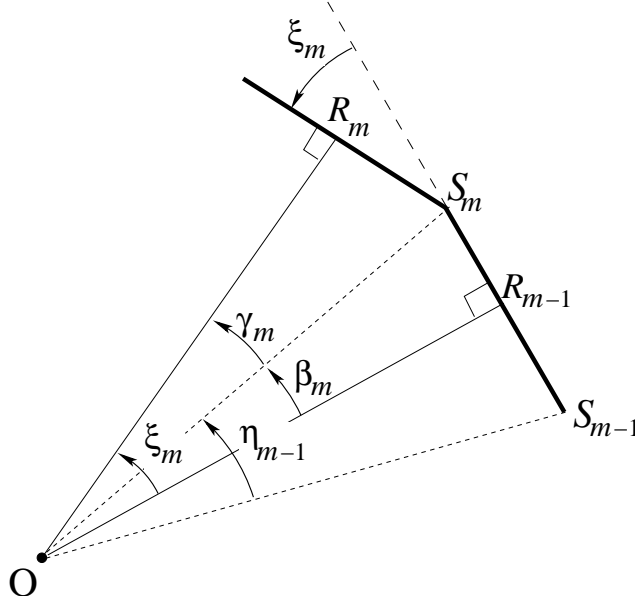


Figure 8: Definition ( $n$ -cyclic in the index  $m$ ) of the angles of integration  $\xi_m$  and  $\eta_m$  and of the auxiliary angles  $\beta_m$  and  $\gamma_m$ .

All seeds other than the  $n$  first neighbors must stay outside the disk of radius  $P$ , which happens with probability  $\exp(-\rho\pi P^2)$ . Hence, extracting a scale factor  $P$  from all  $2n$  position variables in the integration (4.1), we have

$$I_{\text{rad}} = \rho^n \int_0^\infty dP P^{2n-1} e^{-\rho\pi P^2} = \frac{(n-1)!}{2\pi^n}. \quad (4.3)$$

When this integral is performed, the seed density  $\rho$  disappears from the expression for  $p_n$ , as it had to.

The integral  $I_{\text{ang}}$  in (4.2) requires more discussion. It involves  $2n - 1$  dimensionless variables of integration for which we can take any set of  $2n - 1$  independent angles. Introducing an extra factor  $(n-1)!$  allows us to order the  $n$  seeds such that their indices correspond to increasing polar angles. A natural choice of angles is shown in Fig. 8: it is the set of polar angle differences  $\{\xi_m, \eta_m\}$ , where  $\xi_m$  is the angle between two successive mid-point vectors  $R_{m-1}$  and  $R_m$ , and  $\eta_m$  the angle between two successive vertex vectors  $S_m$  and  $S_{m+1}$ .

Fig. 8 also illustrates how the perimeter segments may be constructed successively when the  $\xi_m$  and  $\eta_m$  are given. Two types of construction steps alternate. First, given  $S_{m-1}$  and a direction of departure, continue along this direction until the segment  $S_{m-1}S_m$  spans the angle  $\eta_{m-1}$ ; secondly, when arriving at  $S_m$ , define a new direction of departure by taking an angle of  $\xi_m$  to the left. Iterate  $n$  times.

It is easy to introduce the  $\xi_m$  into (4.1) by passing to a polar coordinate representation for the  $\mathbf{P}_m$ ; however, the passage from the ratios  $P_m/P_{m-1}$  to the  $\eta_m$  leads to the appearance of a nontrivial Jacobian that we will consider now. It follows from Fig. 3 and Fig. 8, where we have introduced an auxiliary angle  $\beta_m$ , that

$$\frac{P_m}{P_{m-1}} = \frac{|OR_m|}{|OR_{m-1}|} = \frac{\cos(\xi_m - \beta_m)}{\cos \beta_m} = \cos \xi_m - \sin \xi_m \tan \beta_m. \quad (4.4)$$

Fig. 8 shows that the angles  $\eta_{m-1}$  and  $\beta_m$  vary with the position of  $S_m$  at a common rate. To find the Jacobian we therefore calculate the derivative

$$\frac{d(P_m/P_{m-1})}{d\eta_{m-1}} = \frac{\sin \xi_m}{\cos^2 \beta_m} \simeq \xi_m, \quad (4.5)$$

the last equality being valid asymptotically for small  $\xi_m$  and  $\beta_m$ , which is the relevant limit when  $n$  gets large. By going around the perimeter one thus finds that the transformation from the  $P_m/P_{m-1}$  to the  $\eta_m$  is accompanied by a Jacobian  $\xi_1 \xi_2 \dots \xi_n$ . This result quantifies our observation at the end of section 3.1, namely that there is an effective repulsion between the mid-points.

The integral on the angular variables now becomes

$$I_{\text{ang}} = (n-1)! I_{\text{vert}} I_{\text{midp}}, \quad (4.6)$$

in which

$$I_{\text{vert}} = \int_0^{2\pi} d\eta_1 \dots d\eta_n \delta \left( \sum_{m=1}^n \eta_m - 2\pi \right) = \frac{(2\pi)^{n-1}}{(n-1)!}, \quad (4.7)$$

$$I_{\text{midp}} = \int_0^{2\pi} d\xi_1 \dots d\xi_n (\xi_1 \dots \xi_n) \delta \left( \sum_{m=1}^n \xi_m - 2\pi \right) = \frac{(2\pi)^{2n-1}}{(2n-1)!}, \quad (4.8)$$

where the delta functions enforce obvious sum rules. Due to these constraints the angles  $\xi_m$  and  $\eta_m$  will typically take values of order  $n^{-1}$  with average  $2\pi/n$ . The exact value (here  $2\pi$ ) of the upper integration limits in (4.7) and (4.8) does not affect the outcome of the integrals to the order in  $n$  that is relevant for our discussion.

## 4.2 Improved result

We now know all the factors that go into the final result. Substituting (4.7) and (4.8) in (4.6) and using the result together with (4.3) in (4.2) gives

$$\begin{aligned} p_n &= \frac{1}{n!} \times (n-1)! \times \frac{(n-1)!}{2\pi^n} \times \frac{(2\pi)^{n-1}}{(n-1)!} \times \frac{(2\pi)^{2n-1}}{(2n-1)!} \\ &= \frac{1}{4\pi^2} \frac{(8\pi^2)^n}{(2n)!}. \end{aligned} \quad (4.9)$$

This improved estimate for  $p_n$  is the end result of this section. The same expression occurred at an intermediate stage of the calculation in Ref. [5], where it went by the name of  $p_n^{(0)}$ . Eq. (4.9) has the  $n$  dependence that we know is exact: upon taking the logarithm we now recover the first three terms of expansion (1.2). The exponential  $(8\pi^2)^n$  and the factorial denominator in (4.9) are therefore correct. However, our derivation has been too crude [33] that we may trust the proportionality constant  $(4\pi^2)^{-1}$ . This constant turns out to differ from the correct one appearing in (1.1) by the factor  $C$ . In the next section we will briefly discuss the origin of this factor.

## 5 Elastic deformations and Gabriel neighbors

In the preceding section we used that the cell perimeter is close to a circle. However, since each of the first-neighbor coordinates  $\mathbf{P}_m$  was integrated over a two-dimensional domain, the integral does not respect this circularity property exactly. This section deals with the deviations from circularity. It will turn out that the quantitative effect of these deviations on the sidedness  $p_n$  is beyond the heuristic approach of this paper.

### 5.1 Random acceleration process

In this subsection  $\mathbf{R}_m$  will denote the position vector of the  $m$ th mid-point and  $R_m \equiv |\mathbf{R}_m|$  its length, for  $m = 1, 2, \dots, n$ . The ratio between two successive mid-point distances can be expressed as  $R_m/R_{m-1} = \cos \gamma_m / \cos \beta_m$ , with the auxiliary angles  $\beta_m$  and  $\gamma_m$  defined in Fig. 8. Hence

$$\frac{R_{m-1}R_{m+1}}{R_m^2} = \frac{\cos \beta_m \cos \gamma_{m+1}}{\cos \gamma_m \cos \beta_{m+1}}. \quad (5.1)$$

We set

$$R_m = R_c + \delta R_m, \quad (5.2)$$

where  $R_c = R^*$  is given by (3.8), and expand both sides of Eq. (5.1) using that  $\beta_m$ ,  $\gamma_m$ , and  $\delta R_m/R_c$  are all small as  $n$  gets large. To leading order this yields the second-order difference equation

$$\begin{aligned} \delta R_{m-1} - 2\delta R_m + \delta R_{m+1} &= -\frac{1}{2}R_c (\beta_m^2 - \gamma_m^2 + \gamma_{m+1}^2 - \beta_{m+1}^2) \\ &= -\frac{1}{2}R_c [\xi_m(\beta_m - \gamma_m) - \xi_{m+1}(\beta_{m+1} - \gamma_{m+1})], \end{aligned} \quad (5.3)$$

where we made use of the identity  $\beta_m + \gamma_m = \xi_m$ . In the second line of (5.3) the differences  $\beta_\ell - \gamma_\ell$  (with  $\ell = m, m+1$ ) are of zero average. In that line we now replace  $\xi_m$  and  $\xi_{m+1}$  by their average  $2\pi/n$ , the idea being that

the random contribution to these angles will have a negligible effect when Eq. (5.3) is integrated (that is, summed on  $m$ ) [34]. The right hand side of Eq. (5.3) having thus become linear in the angles, it appears that we can express the sum of the  $\beta$ 's and  $\gamma$ 's again in terms of the  $\xi$ 's and  $\eta$ 's. In that way we obtain

$$\delta R_{m-1} - 2\delta R_m + \delta R_{m+1} = \frac{\pi^{\frac{1}{2}}}{(\rho n)^{\frac{1}{2}}} F_m \quad (5.4)$$

with

$$F_m = \eta_m - \frac{1}{2}(\xi_m + \xi_{m+1}). \quad (5.5)$$

The left hand side of Eq. (5.4) represents the “radial acceleration” of the perimeter as it turns around the central seed. The right hand side is a random term of known properties. An equation like (5.4) also appeared in Refs. [5] and [13], where the conditions of its validity were discussed. It was shown there that in the limit  $n \rightarrow \infty$ , with the replacement  $m \mapsto \phi \equiv 2\pi mn^{-1}$ , the equation becomes a second-order differential equation  $d^2\delta R(\phi)/d\phi^2 = F(\phi)$  where  $F(\phi)$  is Gaussian noise. For white Gaussian noise this equation is referred to as the *random acceleration process* [19, 20, 18].

For our present discussion Eq. (5.4) suffices as it stands. The key point is that  $F_m$  and  $F_{m'}$  are essentially uncorrelated when  $|m - m'| \geq 2$ . “Essentially” here and below will mean: neglecting the weak anticorrelation, of relative order  $\mathcal{O}(n^{-1})$ , induced by the delta function constraint in the integral in (4.8). The  $F_m$  have zero mean and are, just like the  $\xi_m$  and the  $\eta_m$ , of order  $n^{-1}$  as  $n$  gets large.

Let us now sum both sides of (5.4) from  $m = 1$  to some value of  $m$  which is of order  $n$ . The right hand side becomes a sum of  $\mathcal{O}(n)$  zero-mean and essentially uncorrelated terms that are each of order  $n^{-1}$ ; hence it will be of order  $n^{-\frac{1}{2}}$ . Taking also into account the prefactor  $(\pi/\rho n)^{\frac{1}{2}}$  we find for the “radial speed”  $\delta R_{m+1} - \delta R_m$  of the perimeter the expression

$$(\delta R_{m+1} - \delta R_m) - (\delta R_1 - \delta R_0) = \mathcal{O}(n^{-1}). \quad (5.6)$$

Since the average speed must be zero, this means that also  $\delta R_{m+1} - \delta R_m = \mathcal{O}(n^{-1})$ .

Being the sum of essentially independent increments, the radial speed  $\delta R_{m+1} - \delta R_m$  varies with  $m$  as a random walk trajectory. Such a trajectory has strong long-range correlations. Therefore, if we sum (5.6) once more over  $\mathcal{O}(n)$  values of the index  $m$ , we obtain the sum of  $\mathcal{O}(n)$  strongly correlated terms that are each of order  $n^{-1}$ , which yields

$$\delta R_m - \delta R_1 = \mathcal{O}(1). \quad (5.7)$$

We have argued in section 3.2 that the cell perimeter is contained in an annulus of width  $\sim n^{-\frac{3}{2}}$ . Eq. (5.7) now shows that this annulus is not strictly



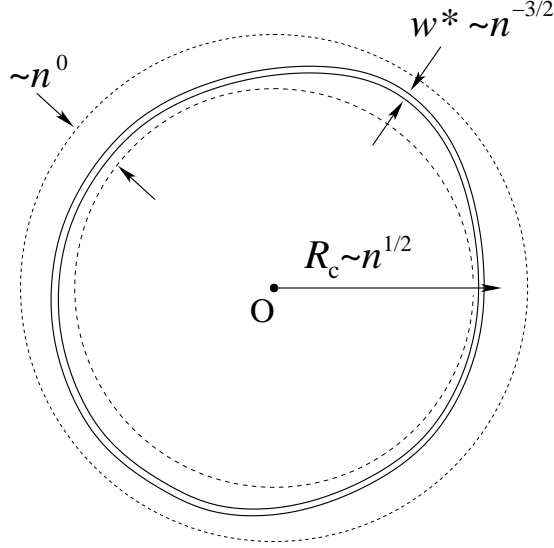


Figure 9: Pair of solid lines: the narrow annulus of width  $w^* \sim n^{-3/2}$  through which the cell perimeter runs. Its radius has variations of order  $n^0$  with respect to an average radius  $R_c \sim n^{1/2}$  and stays, typically, between the two concentric dashed circles.

circular but that its radius deviates from the typical value  $R_c = (n/4\pi\rho)^{1/2}$  by amounts of order unity. In full coherence with this, an evaluation of the radial integral (4.3) by the steepest descent method yields a peak width also of order unity. The resulting large-scale behavior of the cell perimeter has been schematized in Fig. 9. A “real-life” example of a not-quite-circular cell is provided by Fig. 7.

## 5.2 Origin of the constant $C$

In section 5.1 we identified the random acceleration process as the mechanism that governs the perimeter’s deviations from circularity. These deformations may be referred to as “elastic,” with the understanding that this elasticity is of purely entropic origin. It is in fact a long-range, “macroscopic” elasticity that comes over and above the short-range perimeter fluctuations already taken into account in section 4 by the integrations on the  $\xi_m$  and  $\eta_m$ .

The exact determination of the effect on  $p_n$  of these elastic deformations is beyond the heuristic arguments of this paper. For completeness we recall that they may be treated [4, 5] as a superposition of independent Fourier components with wavenumbers  $q = \pm 1, \pm 2, \dots$ . Their amplitudes  $\psi_q$  are Gaussian random variables and their elastic energy [29]  $E = \pi \sum_q \Lambda_q \psi_q \psi_{-q}$  has the dispersion relation

$$\Lambda_q = 1 - q^{-2} + 4q^{-4}. \quad (5.8)$$

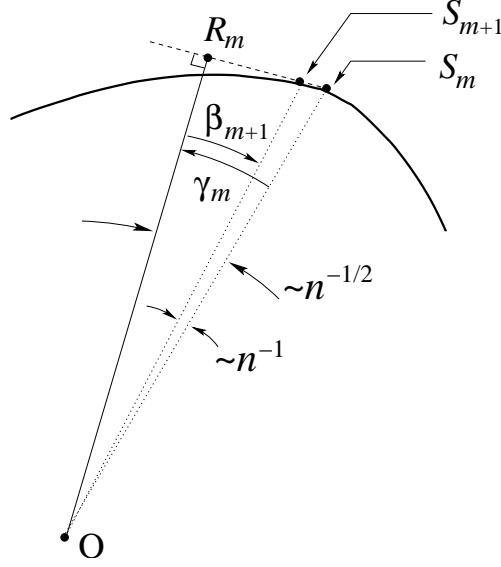


Figure 10: A cell perimeter (heavy solid line) for which the mid-point  $R_m$  does not lie on the  $m$ th perimeter segment  $S_m S_{m+1}$  but elsewhere on the line prolonging this segment. The angle  $\beta_{m+1}$  is negative. The  $\gamma_m$  and  $\beta_m$  are typically of order  $n^{-\frac{1}{2}}$  and the situation depicted in this figure is generic rather than exceptional.

The elastic deformations multiply  $p_n$  by an extra contribution equal to their partition function  $C$ , which is obtained as  $C = \prod_{q=1}^{\infty} \Lambda_q^{-1}$ .

### 5.3 Gabriel neighbors of the many-sided cell

In this subsection we apply the heuristic arguments developed above to Gabriel neighborhood. Two adjacent Voronoi cells are called Gabriel (or full) neighbors if the line segment connecting their seeds does not intersect any other cell. In the notation of this work, the condition for the  $m$ th first neighbor of the central seed to be a Gabriel neighbor is that the mid-point  $R_m$  lie on the perimeter segment  $S_m S_{m+1}$ . In the example of Fig. 10 the  $m$ th neighbor is *not* Gabriel. Reasons for being interested in Gabriel neighbors have been mentioned in the Introduction.

Whereas in two dimensions the average *total* number of neighboring cells is exactly  $\langle n \rangle = 6$ , the average number of full neighbors is equal only to  $\langle n \rangle^{\text{full}} = 4$ . We ask now: given an  $n$ -sided cell, what is its average number  $\nu_n^{\text{full}}$  of Gabriel neighbors? The large- $n$  behavior of  $\nu_n^{\text{full}}$  can be estimated as follows.

Fig. 10 shows that  $R_m$  is in the interval  $S_m S_{m+1}$  if and only if  $\gamma_m$  and  $\beta_{m+1}$  are both positive. These conditions are not independent since  $\gamma_m + \beta_{m+1} = \eta_{m+1}$  and  $\eta_{m+1}$  is necessarily positive. An equivalent condition for the  $m$ th first neighbor to be Gabriel is that  $\gamma_m > 0$  and  $\eta_m > \gamma_m$ . The advantage of

this formulation is that  $\gamma_m$  and  $\eta_m$  are essentially independent (in the same sense as before); this is also clear from the algorithm described in section 4 by which the perimeter is constructed on the basis of given sets of  $\xi$ 's and  $\eta$ 's. Let us write  $w_n(\gamma_m)$  and  $v_n(\eta_m)$  for the probability distributions of the  $\gamma_m$  and the  $\eta_m$ , respectively. We then have

$$\nu_n^{\text{full}} = n \int_0^\infty d\gamma w_n(\gamma) \int_\gamma^\infty d\eta v_n(\eta), \quad (5.9)$$

in which the prefactor  $n$  comes from the total number of cell sides and the remaining integral represents the probability that  $\gamma_m, \beta_{m+1} > 0$ . We now need the distributions  $v_n$  and  $w_n$ . Eq. (4.7) shows that the  $\eta_m$  define the partition of a circle into  $n$  random and independent intervals of average length  $2\pi/n$ . Hence  $v_n(\eta)$  is an exponential of average  $2\pi/n$ ,

$$v_n(\eta) = (n/2\pi)^{-1} \exp(-n\eta/2\pi). \quad (5.10)$$

In order to find  $w_n$  we remark that any difference  $\gamma_{m_2} - \gamma_{m_1}$  can be written as  $\gamma_{m_2} - \gamma_{m_1} = \sum_{m=m_1+1}^{m_2} (\xi_m - \eta_{m-1})$ , which is a sum of  $2m_2 - 2m_1$  essentially independent random variables. It follows that the differences  $\gamma_{m_2} - \gamma_{m_1}$ , as well as the  $\gamma_m$  themselves, are Gaussian distributed with a root-mean-square width that scales as  $n^{-\frac{1}{2}}$ . Knowing that the  $\gamma_m$  must have average  $\pi/n$  and writing the asymptotic behavior of their variance as  $\simeq (c_0 n)^{-1}$  with  $c_0$  a numerical constant, we have that in the large- $n$  limit

$$w_n(\gamma) = (c_0 n/2\pi)^{\frac{1}{2}} \exp\left[-\frac{1}{2}c_0 n(\gamma - \pi/n)^2\right]. \quad (5.11)$$

Of course the angles  $\beta_m$ , related to the  $\gamma_m$  by inversion of the orientation of the perimeter, also have the distribution  $w_n$ . We refer again to Fig. 10 for an additional remark. Since  $w_n$  is a distribution on the scale  $n^{-\frac{1}{2}}$  but the angles  $S_m O S_{m+1} = \eta_m$  are of order  $n^{-1}$ , the situation depicted in this figure is generic: the perpendicular from the origin onto the line containing a perimeter segment will typically hit that line in a point *outside* that segment.

Substituting (5.10) and (5.11) in (5.9) and evaluating in the limit of large  $n$  we obtain the scaling with  $n$  of the number of Gabriel neighbors,

$$\nu_n^{\text{full}} \simeq (2\pi c_0 n)^{\frac{1}{2}}, \quad n \rightarrow \infty. \quad (5.12)$$

This confirms that for many-sided cells Gabriel neighbors are *atypical*. The proportionality constant  $c_0$  in (5.12) cannot be obtained by the present heuristic arguments; it is, however, in principle accessible by a detailed calculation in which, again, the  $\Lambda_q$  will intervene.

## 6 Conclusion

We have developed heuristic arguments applicable to Voronoi cells and whose validity is confirmed by existing exact calculations. The arguments, which

concern Voronoi cells in the limit of large sidedness, are based on the estimation of the entropy of a set of points arranged in a plane under specific geometrical constraints. The power as well as the limitations of these arguments have been indicated. As a new result we have determined by the reasoning of the present paper the asymptotic  $n$  dependence of the average number of Gabriel neighbors of the  $n$ -sided cell.

We may henceforth apply these heuristic methods with a certain confidence in other contexts where no exact calculations are possible. Examples of related problems in mathematics and statistical physics have been mentioned in the Introduction. Finally, this work provides the tools that will be used in an upcoming study of Voronoi cells in higher spatial dimensions.

## References

- [1] A. Okabe, B. Boots, K. Sugihara, and S.N. Chiu, *Spatial tessellations: concepts and applications of Voronoi diagrams*, second edition (John Wiley & Sons Ltd., Chichester, 2000).
- [2] N. Rivier, in *Disorder and Granular Media*, eds. D. Bideaux and A. Hansen (Elsevier, Amsterdam 1993).
- [3] J.L. Meijering, *Philips Research Reports* **8**, 270 (1953).
- [4] H.J. Hilhorst, *J. Stat. Mech.* L02003 (2005).
- [5] H.J. Hilhorst, *J. Stat. Mech.* P09005 (2005).
- [6] Eqs. (1.1) and (1.2) are exact by the usual standards of mathematical physics; however, they are still awaiting rigorous mathematical confirmation.
- [7] H.J. Hilhorst, *J. Phys. A* **39**, 7227 (2006).
- [8] D.A. Aboav, *Metallography* **3**, 383 (1970).
- [9] H.J. Hilhorst, *J. Phys. A* **40**, 2615 (2007).
- [10] The accuracy of earlier Monte Carlo methods [31, 32] is down to the single-digit level when  $n \approx 20$ .
- [11] H.J. Hilhorst and P. Calka, *J. Stat. Phys.* **132** (2008) 627.
- [12] D. Hug and R. Schneider, *Geom. Funct. Anal.* **17**, 156 (2007).
- [13] H.J. Hilhorst, P. Calka, and G. Schehr, *J. Stat. Mech.* (2008) P10010.

- [14] J.J. Sylvester, Problem 1491, *The Educational Times* (April 1864), London.
- [15] I. Bárány, *The Annals of Probability* **27**, 2020 (1999).
- [16] I. Bárány, G. Rote, W. Steiger, and C.-H. Zhang, *Discrete Comput. Geom.* **23**, 35 (2000).
- [17] P. Calka and T. Schreiber, *Ann. Probab.* **33**, 1625 (2005).
- [18] G. Györfyi, N.R. Moloney, K. Ozogány, and Z. Rácz, *Phys. Rev. E* **75**, 021123 (2007).
- [19] S. Majumdar and A. Comtet, *Phys. Rev. Lett.* **92**, 225501 (2004).
- [20] S. Majumdar and A. Comtet, *J. Stat. Phys.* **119**, 777 (2005).
- [21] H.J. Hilhorst, unpublished.
- [22] J. Møller, *Lectures on Random Voronoi Tessellations*. Lecture Notes in Statistics, Vol. 87 (1994), Springer, New York.
- [23] J. Møller and D. Stoyan, *Stochastic Geometry and Random Tessellations* preprint 2007. To appear in: “Tessellations in the Sciences: Virtues, Techniques and Applications of Geometric Tilings”, eds. R. van de Weijgaert, G. Vegter, V. Icke, and J. Ritzerveld. Springer Verlag.
- [24] B. Bhattacharya, K. Mukherjee, and G. Toussaint, in: *Pattern Recognition and Machine Intelligence*, pp.60-69, Lecture Notes in Computer Science, Vol. 3776 (2005), Springer Berlin / Heidelberg.
- [25] H. Chen and W. Wei, in: *Intelligent Computing in Signal Processing and Pattern Recognition*, pp. 882-887, Lecture Notes in Control and Information Sciences, Vol. 345 (2006), Springer Berlin / Heidelberg.
- [26] For cells whose area becomes large, approach to circularity was originally conjectured by Kendall in the early 1940’s. This was subsequently confirmed by various mathematical proofs due to Calka and Schreiber [17] and Hug *et al.* [27, 12].
- [27] D. Hug, M. Reitzner, and R. Schneider, *Adv. in Appl. Probab.* **36**, 667 (2004).
- [28] P. Calka, *Adv. in Appl. Probab.* **34**, 702 (2002).
- [29] In analogy with many other problems in statistical physics, if  $p$  is a phase space integral we will sometimes imagine it written as  $p = e^S$  and call  $S$  an entropy, or as  $p = e^{-E}$  and call  $E$  an energy.

- [30] H.J. Hilhorst, in: Proceedings of STATPHYS 23, Genoa, Italy, July 9-13, 2007. *European Physical Journal B* **64**, 437 (2008).
- [31] J.M. Drouffe and C. Itzykson, *Nuclear Physics B* **235** [FS11], 45 (1984).
- [32] C. Itzykson and J.M. Drouffe, *Statistical Field Theory*, Vol. 2 (Cambridge University Press, Cambridge 1989), chapter 11.
- [33] In fact, in (4.9) a cancellation has occurred between two factors of distinct origin that we did not take into account in the argument of section 4. First, a trivial factor  $2\pi$  comes from the rotational degree of freedom of the cell. Secondly, a factor  $(2\pi)^{-1}$  has a more subtle origin: it arises from an extra nonlinear constraint on the  $\xi_m$  and  $\eta_m$ , needed to guarantee that the perimeter closes onto itself after turning around the central seed.
- [34] Correlations between the  $\beta_\ell$  and  $\gamma_\ell$  on the one hand and the  $\xi_m$  and  $\eta_m$  on the other, are negligible in the large- $n$  limit.